

JAAS

Accepted Manuscript



This is an *Accepted Manuscript*, which has been through the Royal Society of Chemistry peer review process and has been accepted for publication.

Accepted Manuscripts are published online shortly after acceptance, before technical editing, formatting and proof reading. Using this free service, authors can make their results available to the community, in citable form, before we publish the edited article. We will replace this *Accepted Manuscript* with the edited and formatted *Advance Article* as soon as it is available.

You can find more information about *Accepted Manuscripts* in the [Information for Authors](#).

Please note that technical editing may introduce minor changes to the text and/or graphics, which may alter content. The journal's standard [Terms & Conditions](#) and the [Ethical guidelines](#) still apply. In no event shall the Royal Society of Chemistry be held responsible for any errors or omissions in this *Accepted Manuscript* or any consequences arising from the use of any information it contains.

ARTICLE

in situ monitoring of corrosion processes by coupled micro-XRF/micro-XRD mapping to understand degradation mechanisms of reinforcing bars in hydraulic binders from historical monuments

Cite this: DOI: 10.1039/x0xx00000x

Received 00th January 2012,

Accepted 00th January 2012

DOI: 10.1039/x0xx00000x

www.rsc.org/S. Grousset^a, F. Kergourlay^b, D. Neff^a, E. Foy^a, J.-L. Gallias^b, S. Reguer^c, P. Dillmann^a, A. Noumowé^b

Historic monuments have been partly built since the Antiquity with iron or steel reinforcement sealed in mortars or hydraulic binders. But the presence of chloride in the environment can weaken the structures due to the corrosion of these metallic parts, leading to the cracking of the binder. In this context, in order to better understand the first steps of these corrosion mechanisms a chemical cell has been designed to operate in-situ analyses of the phases precipitated when a chlorinated solution is introduced at the vicinity of the bar. For that chemical and structural characterisation (micro-XRF and micro-XRD respectively) has been performed under synchrotron radiation on Soleil-DiffAbs beamline. Moreover complementary SEM-EDS analyses have been carried out before and after the in-situ cell experiment in order to determine the final localisation inside the crack network of the corrosion products. The results show first that iron can spread up to 1 mm of the metallic bar inside the pores of the binder after 44h of corrosion. Moreover, in accordance with laboratory experiments conducted in solution in presence of Fe²⁺ and Cl⁻ ions the reaction pathways conduct to the successive formation of an intermediate Fe(II)-Fe(III) chlorinated green rust which transforms in ferric oxyhydroxydes such as akaganeite or goethite depending on the local concentration of iron.

Introduction

Since several centuries, historic monuments have been reinforced by the use of iron or steel bars embedded in binders such as lead, plasters, mortar or concrete. In fact the earliest use of metal to reinforce monuments date from Antiquity. Since, construction techniques have evolved but metal has never ceased to be employed in the building^{1,2}. During last centuries, many historic monuments have been reinforced by the use of iron or steel bars embedded in mortar or concrete made with hydraulic binders. This is the case for example at the Popes Palace of Avignon (14th c.)³ where tons of metals were employed or at façade of the Saint-Gervais Saint-Protais (17th c.) church in Paris. A more recent use of metal in the historical building can be found in the monuments of the beginning of the 20th c. made of reinforced concrete⁴. However, architects and conservators draw up an alarming report concerning built heritage preservation. In particular, damages due to corrosion of iron reinforcement in these binders are critical. The degradation of the monument is visible toward the cracking and spalling of binder.⁵⁻⁷

In order to overcome such problems, the conservation approach consists in three main lines of action: first the identification of the conservation state, then the prediction of the iron corrosion and last the development of adapted conservation strategies⁸.

The corrosion processes of reinforced concrete and hydraulic binders are explained by a variation of the chemical conditions. The initial alkaline conditions within binders allow the formation of a passive and protective layer on iron avoiding further corrosion. However a decrease of the solution pH during binder carbonation⁹, and/or the progression of aggressive chemical species such as chloride ions towards the reinforcement¹⁰, can lead to the destabilization of the passive layer and let corrosion occur. Corrosion processes imply the formation of corrosion products which can generate crack and binder spalling caused by high tensile stresses generated in the medium^{11,12}.

In particular laboratory experiments on steel bars corroded in a chlorinated concrete under various conditions have shown that the corrosion layers observed were mainly composed of non-chlorinated phases, magnetite (Fe₃O₄) and goethite (α -FeOOH). However Cl-containing phases like the ferrous hydroxychloride β -Fe₂(OH)₃Cl was observed only deep in the needle-like pits¹³. Although it is well known that chloride ions participate in the steel depassivation leading to pit formation, their role in the advanced stages of iron corrosion in binders is not well understood¹⁴. Especially it was supposed that transient phases of lower density form, causing an increase of the binder cracking phenomenon¹⁵.

The aim of the present study is to better understand the first steps of corrosion processes occurring on steel reinforcement in

mortar exposed to chlorinated environments in order (i) to determine the location of the corrosion processes (ii) to identify the transient corrosion products and their evolution with time: the role of intermediate iron corrosion products, particularly chlorine-containing ones has to be revealed and (iii) to highlight the physico-chemical conditions allowing the ferrous species transport within the binder porous system. Previous in-situ studies have highlighted thanks to X-ray fluorescence that diffusion of elemental iron among other elements can be followed on several hours^{16, 17}. In the present study a combination of X-ray fluorescence and diffraction was designed in order to collect both composition and chemical structure of the phases formed in-situ at a micrometric scale. In this way, a dedicated cell replicating a steel bar inside a Portland cement mortar has been achieved to perform *in situ* structural and elementary analysis during the corrosion process. The analytical approach proposed here is based on the use of complementary micro-beam techniques delivering data on the local chemical composition and crystalline structure: Scanning Electron Microscope and Energy Dispersive Spectroscopy (SEM-EDS), X-Ray Diffraction and X-Ray Fluorescence spectroscopy using a micro-beam (labelled micro-XRD and micro-XRF respectively), the latter conducted on both laboratory set-up and under synchrotron radiation in order to adjust the time and scale resolution during in-situ experiments. In addition global observations were consigned concerning the diffusion of water and the variation of the pH in order to understand the processes occurring during the experiment.

Methodology and methods

Experimental cells

Cells composed of mortar and steel bare bars have been studied. Mortar has been chosen because of its similarity to materials employed in ancient building¹⁸. Mortar has been prepared with a water/cement ratio of 0.5 and sand/cement ratio of 3 using a CEMI 52.5 N CP2 cement type. The cells were designed following the protocol presented below (Figure 1). First the steel bar ($\Phi=1$ cm, H=12 cm) is maintained vertically at the center of a cylindrical plastic mold ($\Phi=3$ cm, H=12 cm). Along the bar, a multifilament glass yarn ($\Phi=2$ mm, H=12 cm) is fastened. Mortar is cast in the mold and the whole dried during 28 days at ambient conditions. After that the plastic mold is removed, the obtained cylinder embedded in epoxy resin before sections of 1 centimeter thickness are cut with a diamond wheel saw to prepare the cells in cross section mode.

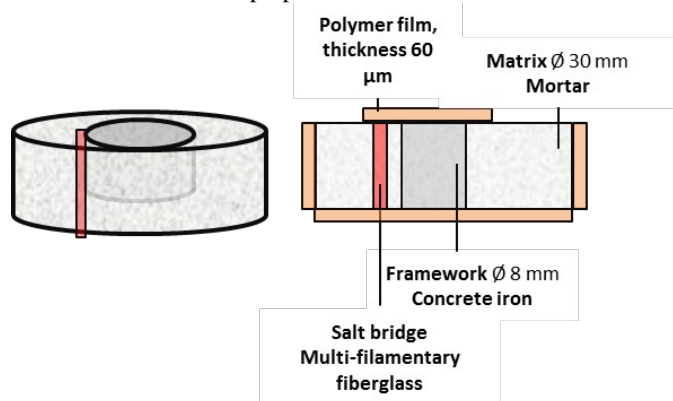


Figure 1: schematic diagram of the in-situ cell, left, perspective view, right, transverse view

Each cross section was prepared as follows: it is first ground with SiC papers and then polish with a 3 μm diamond paste under ethanol. On the front of the cells an adhesive polymer film is applied in order to avoid the air penetration through the observation side, but without obstruction for micro-XRD and micro-XRF analyses. For the experiment the cells were wetted by capillarity through the glass filament trapped in the binder at the vicinity of the steel bar, ensuring a penetration of the chlorinated solution at the binder / iron interface.

A solution of NaCl at 0.5 M concentration was used in order to simulate seashore environment. The solution was injected in the cell thanks to a syringe whose needle was inserted in the multifilament glass yarn at the cells' back until the absorption front appearing in the front of the cell was stabilised.

Analytical methodology was conducted as explained in the following. First at a macroscopic scale a mapping was realized on the front of the cell thanks to SEM-EDS analyses to determine the composition of the major and minor elements around the steel bar. Then the cells were wetted as described above and the penetration of the solution was assessed by macrophotography. In addition the pH change was evaluated thanks to pH papers disposed on the front of the cell. The strong capillary absorption of the chlorinate solution by the multifilament yarn close to the steel bar allows transport of enough chlorinated solution to wet all the interface between mortar and steel bar as shown by visual monitoring of the progression of capillary absorption and create in this way favorable conditions for iron corrosion. The cells were then put on the analytical in-situ set-up to carry out in situ elementary and structural monitoring thanks to the combination of micro-XRD and micro-XRF. The Table 1 summarises the in situ analyses of the three cells presented in this paper. The detailed protocol is described hereafter. The Table 1 summarises the conditions of preparation and analyses of the three cells presented here.

Table 1 : Conditions and duration of in-situ acquisitions

Cell	in-Situ Analyses	Duration of the in situ measurements
C09-C04	micro-XRD + micro-XRF on laboratory set-up	24h
C07-C01	micro-XRD + micro-XRF on laboratory set-up	105h
C02-E03	micro-XRD + micro-XRF, under synchrotron radiation	65h

After the cells were dried in air, SEM-EDS analyses were carried out to determine the precipitation zones of iron phases in the porosities of the mortar / steel interface.

The morphology was observed using optical microscope and SEM (acceleration voltage 15 kV), and compositions were determined by EDS. EDS detection was carried out with a Silicon drift detector allowing to quantify oxygen with an error of 2% and other elements under 0.5 wt.% with 1% of error.

in situ characterization protocol

micro-XRD and micro-XRF were performed on two complementary set-ups. The first one is a laboratory rotating anode that allowed testing the cell design and performing experiments of more than 100 hours. An XRD measurement lasts at least one hour and a half with such disposal. Consequently to determine the first step phases formed during the corrosion process, a shorter acquisition time is needed. That's why a second set-up for *in situ* monitoring of the corrosion layer's structural evolution has been achieved on DiffAbs beamline¹⁹ at Synchrotron SOLEIL. The advantage of such analyses is to acquire XRD and XRF maps in order to locate the phases formed during the corrosion process and show their local heterogeneity.

Setup on Rotating anode X-ray generator

For micro-XRD measurements, a Mo anticathode of a rotating anode X-ray generator delivered a monochromatic beam at 17.48 keV focused to a 50 μm \times 30 μm surface (flux of about 10^6 ph.s⁻¹) using a Xenocs® FOX2D Mo 25_25P diffraction optic (Figure 2). This optic is a curved mirror with graded multilayer coatings that monochromatizes the incident beam from a single reflection. The cells were placed at an angle of 3° from the incident beam in order to work in reflection mode, and the spot size at the sample surface was about 1000 μm (horizontal finger print due to incident angle) \times 30 μm . Diffraction patterns were collected during about 1h30 using a two-dimensional detector (image plate). Data processing was carried out with the EVA software and the ICDD-JCPDS database. XRF was acquired thanks to a Silicon Drift Detector.



Figure 2 : *in situ* setup monitoring, rotating anode X-ray generator; 1. X-ray (Mo, $\lambda_{\text{K}\alpha} = 0,709 \text{ \AA}$), 2. XRF detector, 3. OM, 4. Image plate, 5. Translation table, 6. Chlorinated solution, 7. Cell

DiffAbs beamline at Soleil

The main optical system of DiffAbs beamline consists of a fixed-exit Si(111) double crystal monochromator and provides a sagittal focusing (in the horizontal plane) of the monochromatic beam at 17 keV. In addition, two long mirrors collimate and focus the beam in the vertical plane, allow harmonic rejection and improve energy resolution. A secondary

optical system that consists of two trapezoidal shape flat and orthogonally placed curved mirrors under grazing incidence (in Kirkpatrick Baez geometry) was used for the present experiment to focus the beam down to 10 \times 10 μm^2 with a flux about $10^{10} - 10^{11}$ ph.s⁻¹. The cell has been placed under the beam with an incident angle of 5°, implying beam size finger print about 150 μm \times 10 μm (H \times V fwhm) on the sample.

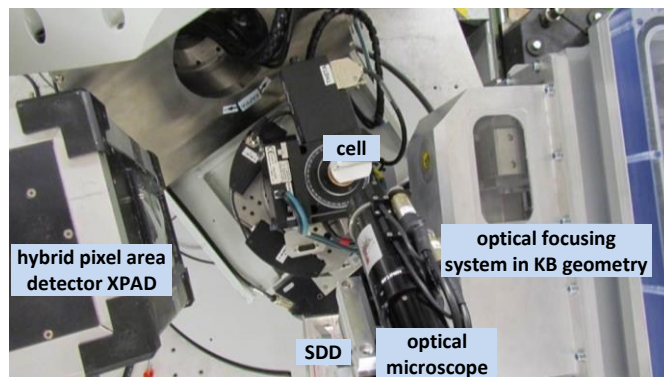


Figure 3 : DiffAbs experimental setup, SOLEIL synchrotron, 1) experimental cell, 2)

A SDD 4Elements detector was used to collect micro-XRF data. In addition, thanks to rapid acquisition obtained by coupling the very great brightness of synchrotron source and the temporal performances of the pixel hybrid XPAD detector²⁰, micro-XRD distribution maps of corrosion products formed during the penetration of the chlorinated solution have been established. The methodology to obtain micro-XRD maps can be described as following:

- An Area Of Interest (AOI) is selected thanks to an optical microscope and XRF measurements, and micro-XRD acquisitions are collected on the AOI thanks to the XPAD detector on a defined dimension. For the studied cell C02-E03, a first map of 1.1 \times 0.9 mm² and after 32h of treatment a second map on a farther 1.1 \times 1.8 mm² extended zone were acquired with a step of 100 \times 30 μm^2 (H \times V) and acquisition time of 10 s/step on the same region during 65h (=80 min/map and 44 maps acquired). Each step contains 1 diffraction image.
- After a set of geometrical and intensities corrections, the diffraction diagrams are obtained from the circular integration of 2D XRD images
- The area evolution of a single diffraction peak per phase is monitored to obtain maps of phases' distribution. Peaks selected for each phase are reported in Table 2.

Table 2 : Diffraction peak and JCPDS file used for the XRD mapping

Phase	JCPDS file	Diffraction peak (hkl)
Akaganeite β -FeOOH	01-080-1770	(101)
Chlorinated green rust $[\text{Fe}^{\text{II}}_3\text{Fe}^{\text{III}}(\text{OH})_8]^+[\text{Cl}.n\text{H}_2\text{O}]^-$	00-040-0127	(006)
Goethite α -FeOOH	00-029-0713	(110)

Results

The penetration of the solution was assessed thanks to macrophotography. This monitoring of the capillary penetration of the chlorinated solution (Figure 4) shows a propagation from the inert multifilament yarn to the binder all around the steel / mortar interface. For the three studied cells the stabilization of the propagation front, i.e. when no macroscopic evolution of the migration front is observed when a drop of solution is added, is comprised between 1 and 4 hours. These different values are due to the variable mortar porosity between the different cells, despite same preparation conditions. The macroscopic cracks present in the cell because of the shrinkage of the mortar during dry curing seem to facilitate the fast and long-distance spreading of the chlorinated solution in the mortar.

The color change of the pH indicator strips placed on the surface of the cell indicates a pH around 13 in the zones saturated by the solution. These initial alkaline conditions were expected since the pore water is in equilibrium with each of the solid phases present in the cementitious material. The chemical maps collected by SEM-EDS on non-treated cross-sections (Figure 6) indicate that initially, except in the metal, iron is not detected on the three cells, even at the vicinity of the steel bar. From these maps, areas were selected for the monitoring of Fe transport by micro-XRF and phase evolution by micro-XRD on the laboratory rotating anode setup. Results obtained in the three cells are very reproducible.

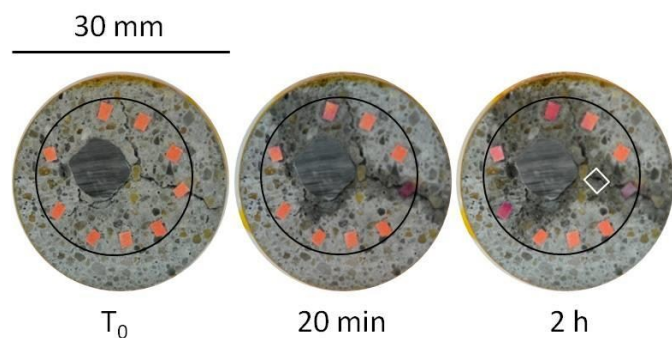


Figure 4: Cell C02-E03, Monitoring of the capillary penetration of a chlorinated solution (0.5M NaCl)

Iron content profiles obtained on the C09-C04 cell at various durations of experiment are presented on Figure 5. The profile obtained at $t=0$ shows the initial location of the rebar. The fact that the decrease does not form a sharp step is due to the size of the beam, enlarged horizontally because of the low incidence angle setup. The 600 μm large beam averages the irregularity of the metal/binder interface. Consequently the part of the profile between 1700 and 1800 μm cannot be considered to study the Fe migration in the binder because it is constituted of a mix of signal coming from the metal, a thin initial corrosion layer, and the binder. For higher distance values, it can be considered that the observations are made in the initial binder as showed by the increase of the Ca content. At these locations, the profile of Fe content obtained at $t=0$ shows the initial distribution of this element in the binder. Fe content is very low (note that the XRF detection limit of iron is of 2 order of magnitude lower than EDS). After 2 hours the Fe content in the binder begins to increase significantly and continuously until the last measurement after 21 hours. For each acquisition time, the profile decreases from the rebar to the outer part of the binder, confirming that the source of the iron is the corrosion of the rebar. Nevertheless, despite this trend, the profiles all show important irregularities. These local increases of the iron content are probably due to larger porosities, and in some case, as for $t=6\text{h}$ and 21h between 2500 and 2800 μm , they can still be filled by corrosion product precipitation. Thus, after 21h, iron has migrated more than 1 mm far from the initial metal/binder interface. Post mortem analyses performed by SEM-EDS (Figure 6) confirm this observation. The migration paths of Fe species in the binder seem to follow in priority the larger cracks and pores. These cracks and pore appear in black before the experiment on Figure 2, at the end of the experiment, they are completely filled with iron corrosion products.

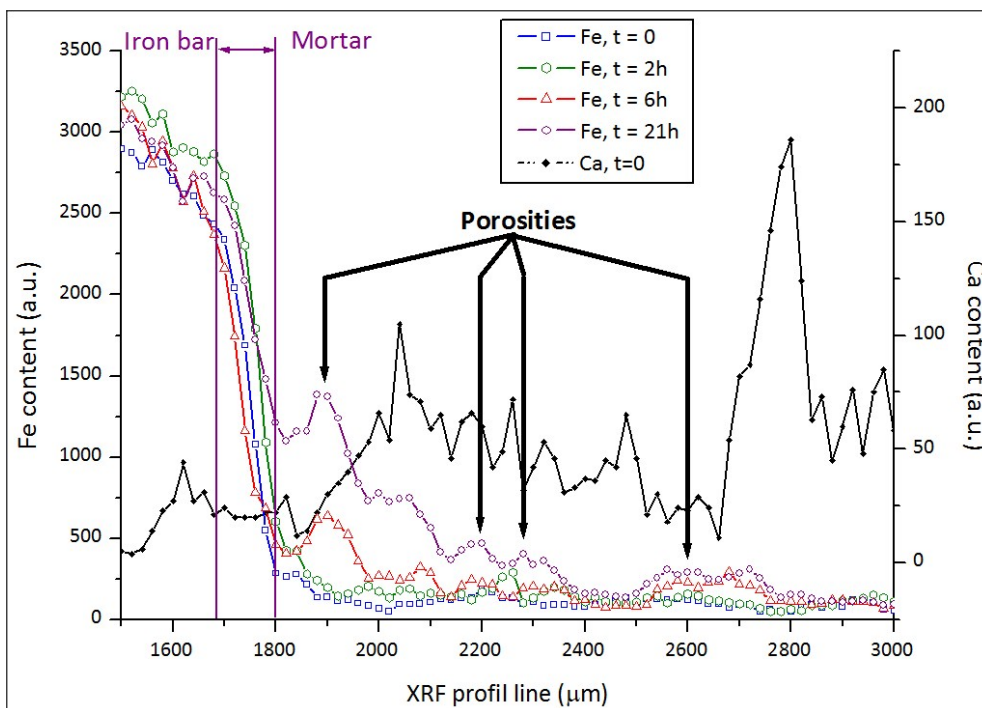


Figure 5 : cell C09-C04, micro-XRF profiles obtained with the laboratory setup

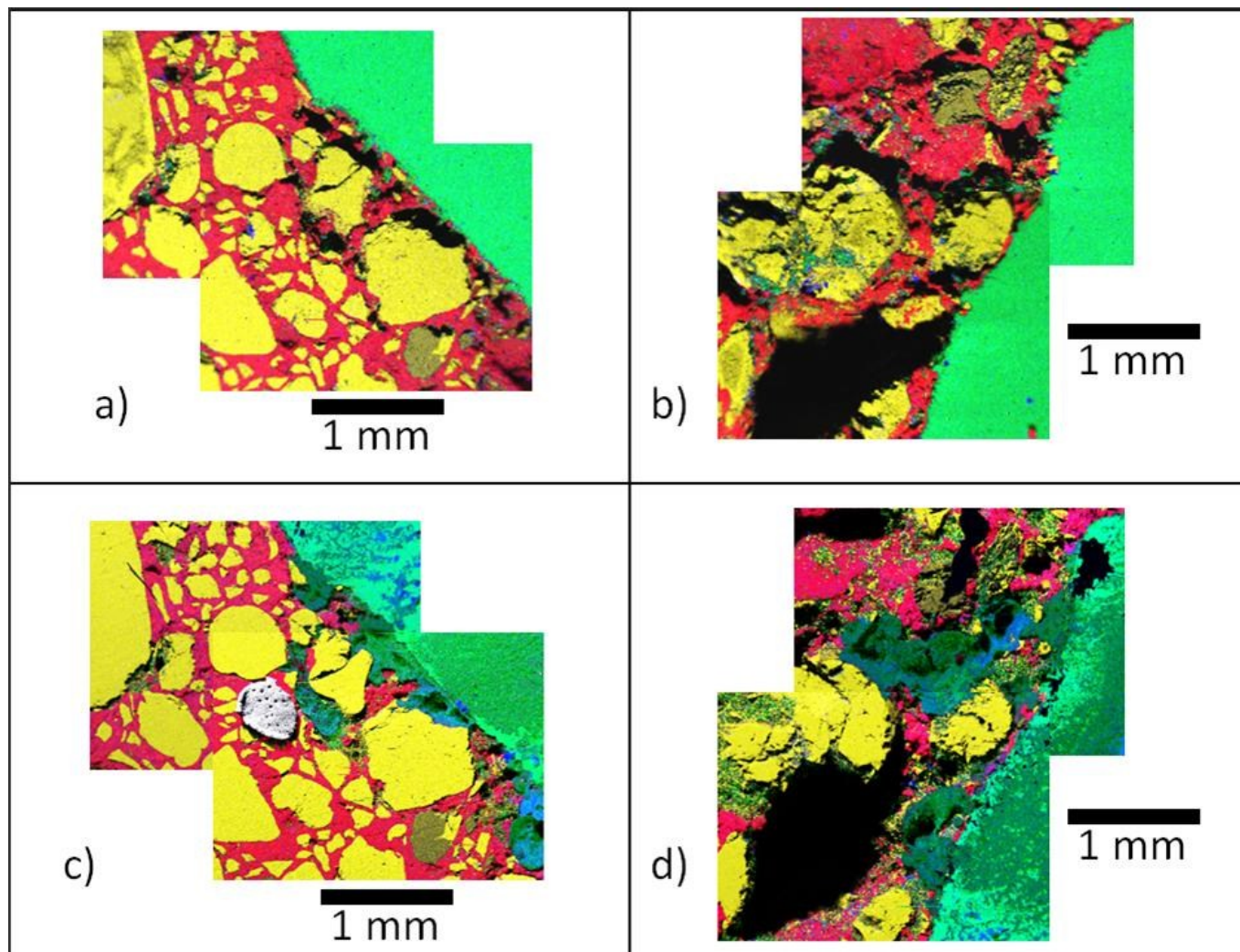


Figure 6 : Cell C02-E03, EDS maps (Fe = green, Ca = red, Si = yellow, Cl = blue): a) & b) Respectively zone 1 & 2 before the corrosion ; c) & d) Respectively zone 1 & 2 after the "in-situ" monitoring of the corrosion process showing the presence of iron inside the cement paste. The gray array on c) is due to an artefact linked to a thick C deposition before SEM observation.

The micro-XRD patterns obtained « in situ » at the distance of 1950 μm during experiment on the laboratory rotating anode setup (Figure 7) show after 7h30 of corrosion, the presence of chlorinated green rust and a minority of akaganeite ($\beta\text{-FeOOH}$). The chlorinated green rust is a compound rarely observed on corrosion products because of its low chemical stability when it is exposed to air and has been mainly studied in laboratory²¹.

While the green rust is the main product at the beginning of the corrosion processes, it seems to progressively disappear in favour of akaganeite. It can be noted that a shoulder at 9.7° appears and could be due to the presence of goethite ($\alpha\text{-FeOOH}$). After 50 hours the peaks of GR are weaker but still present. After 68 hours there is no green rust anymore and akaganeite is the main product detected.

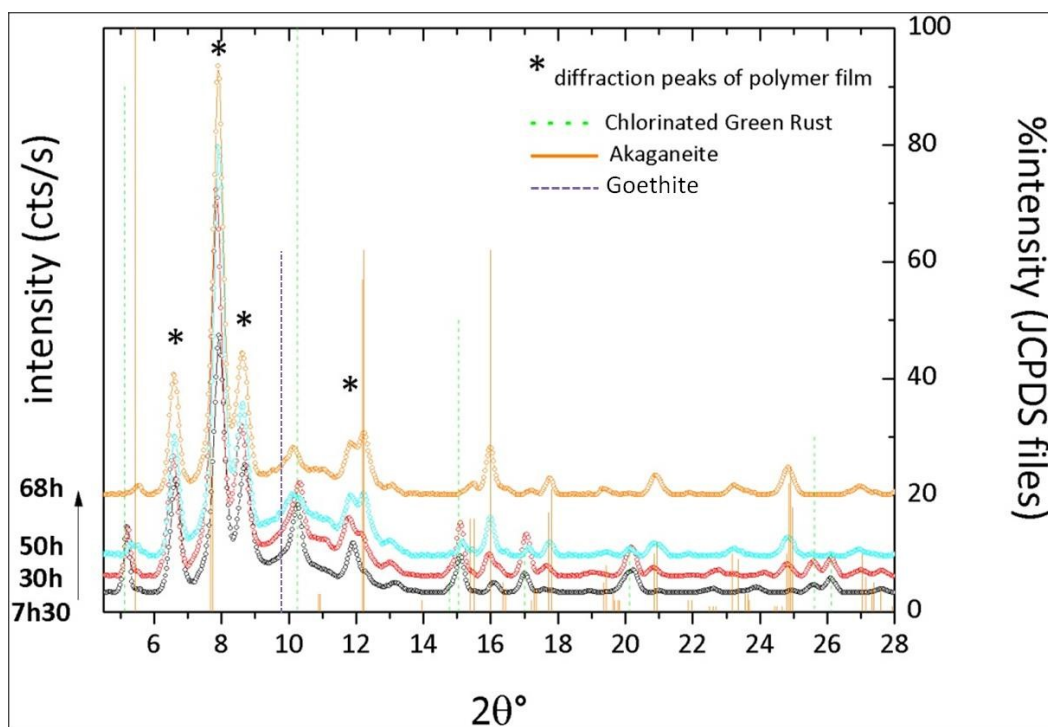


Figure 7: Cell C07-C01, X-Ray diffraction patterns obtained on the laboratory setup from 7h30 to 68h of corrosion

The micro-XRD diffraction maps, obtained on DiffAbs beamline with a much smaller beam than on the laboratory setup, 1h after the beginning of the in situ experiment (Figure 8-1), confirm that the main phase formed near the iron rebar is the chlorinated green rust. At some locations, spots of akaganeite appear. After 4 hours (not shown here) the same observations are noted, with an increase of the intensities for each phases and a spreading of the green rust precipitation zone towards the external zone farther from the iron rebar. The same phenomenon is observed at 8 hours i.e. akaganeite precipitates locally near the bar, green rust zones extends and for both phases an increase of the peak intensities attests of a tendency to higher amounts. But at the same time some goethite appeared at a farther distance of the steel bar. It has to be noted that during

the experiment, it appears that the akaganeite dominance area grows and shifts on the surface of the transverse section of the bars probably due to a local peel off of the adhesive film in contact with the solution. The same observations can be done after 12 and 16 hours of experiment (not shown here). After 20 hours, green rust starts to disappear whereas akaganeite remains present near the metal and goethite at a farther distance of it. After 32h of experiment, the green rust has completely disappeared from the map and the system is stabilized as shown on the 44h maps. The following maps show the presence of goethite from 0.6 to 1.6 millimeter from the steel bar. Thus, chlorinated green rust, akaganeite and goethite could be dominant, simultaneously in different areas, roughly depending on the distance from the metal/binder interface.

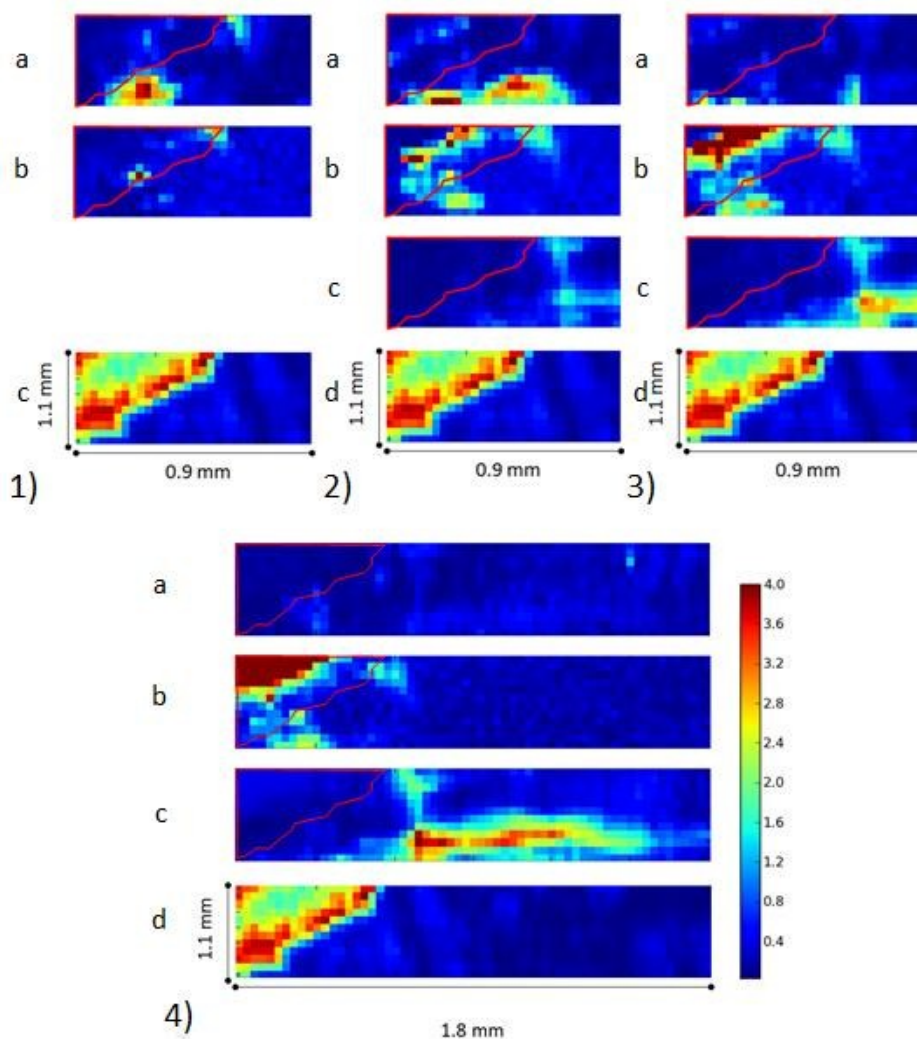


Figure 8 : Cell C02-E03, X-Ray diffraction maps obtained on the DiffAbs beamline at the Synchrotron Soleil : distribution of a) chlorinated green rust ; b) akaganeite ; c) goethite ; d) iron ; after 1) 1h, 2) 8h, 3) 20h and 4) 44h of monitoring.

Discussion

The first step of the experiment is characterized by the capillary penetration of the chlorinated solution. After saturation of the pore network, pH indicators placed on the cell indicates a value of 13. In a first approximation it is representative of the pH of the pore solution imposed by the buffering effect of the binder. Consequently, $[\text{OH}^-] = 0.1 \text{ mol.L}^{-1}$. Moreover, the initial concentration of the NaCl solution is 0.5 mol.L^{-1} and it can be considered that it corresponds to the concentration in the solution saturating the poral network. Last statement, the solution is aerated during all the experiment.

micro-XRF profiles show that, in the conditions of the experiments, the iron corrosion products migrate in the pores of the binder before precipitating. After 21h of corrosion, this migration process allowed significant quantities of iron to be transported at more than 1 mm of the binder/rebar interface. It seems nevertheless as shown on micro-XRD maps that this migration is hindered by phase precipitation: the 40h maps are similar to the 32h ones. To migrate relatively far from the metal/binder interface, iron is dissolved in the pore solution under the form of complexed Fe^{2+} ions at basic pH. Refait et al^{22, 23} and Rémaizeilles et al^{21, 24} studied in different papers the evolution of solutions containing Fe^{2+} and Cl^- compounds that oxidise under aerated conditions. Let us discuss the present results considering these former studies.

These authors discussed the oxidation mechanisms of the Fe(II) containing phases (obtained by mixing NaOH and FeCl₂·4H₂O) in function of two parameters: $R = [\text{Fe}^{2+}]/[\text{OH}^-]$ and $R' = [\text{Cl}^-]/[\text{OH}^-]$. The diagram of Figure 9 sums up a part of these results corresponding to “low” oxidation rates, i.e. without adding of H₂O₂ and obtained in aerated conditions in a stirred solution. First it is interesting to note that despite variations of the stirring rate, the time for oxidizing Fe²⁺ species in aerated conditions is in the same order of magnitude than the one observed in the present study. For example, in ²³ for $R'=3$, it takes about 4 hours to obtain akaganeite from the initial solution. This time increases with R' and can reach sometimes 10 hours. Here, in the pore network of the binder, despite O₂ can access the solution, it is probable that this access is hindered compared to the stirred solution. Thus the oxidation duration to obtain the final product is slightly higher and can reach several 10 hours. However the evolution paths of the phases precipitated in both laboratory or cell conditions are very comparable. In the cell experiment it can be supposed in a first approximation that in the pores $R'=5$ (i.e. $[\text{OH}^-]=0.1\text{ mol}\cdot\text{L}^{-1}$ and $[\text{Cl}^-]=0.5\text{ mol}\cdot\text{L}^{-1}$). The evolution path of the phases for $R' = 5$ shows that the oxidation of Fe²⁺ should first lead to the formation of $\beta\text{-Fe}_2(\text{OH})_3\text{Cl}$ and then to the chlorinated green rust (Fe^{II}₃Fe^{III}(OH)₈[Cl·nH₂O]). The first compound was not observed here: after at least 1 hour, the only detected compound by micro-XRD is the chlorinated green rust. The fact that the first micro-XRD map was acquired 1h after the NaCl introduction could explain the absence of the first transient phase that has already disappeared.

In the following stages of the oxidation process proposed in Figure 9, the green rust progressively transformed into Fe(III)

oxihydroxides. For $R' = 5$ the product are a mix of lepidocrocite ($\gamma\text{-FeOOH}$), goethite ($\alpha\text{-FeOOH}$) and akaganeite ($\beta\text{-FeOOH}$). Actually Refait et al ^{22, 23} indicate that the higher R' is, the less lepidocrocite is observed and the more goethite and akaganeite. This is in relatively good agreement with the observations made by micro-XRD mapping for the present study: after 8h akaganeite and goethite begin to replace green rust. After 22h this latter green rust has quasi totally disappeared and is totally transformed after 32h in both akaganeite and goethite depending on the location towards the steel bar. In the cell in-situ, compared to the oxidation processes observed in the laboratory by Refait, Rémazeilles and co-workers for a $R'=5$, no lepidocrocite is observed. This can be explained by several factors. The first one is that in the cell the dissolved oxygen content could be lower although the conditions are aerated and limit the kinetic of formation lepidocrocite. Moreover for the relatively high R' parameter, not so far from 6 the nature of the final phases is also influenced by the parameter R . During studies presented on Figure 9, R was always fixed at $R'/2$, but other experiments performed by Rémazeilles ²⁴ showed that for a given R' , a decrease of R (i.e. a decrease of $[\text{Fe}^{2+}]$) favours the precipitation of goethite versus akaganeite. This could explain at the same time that precipitation of goethite seems to be more important farther from the metal/binder interface, where the iron concentration is lower, as demonstrated by the XRF profile.

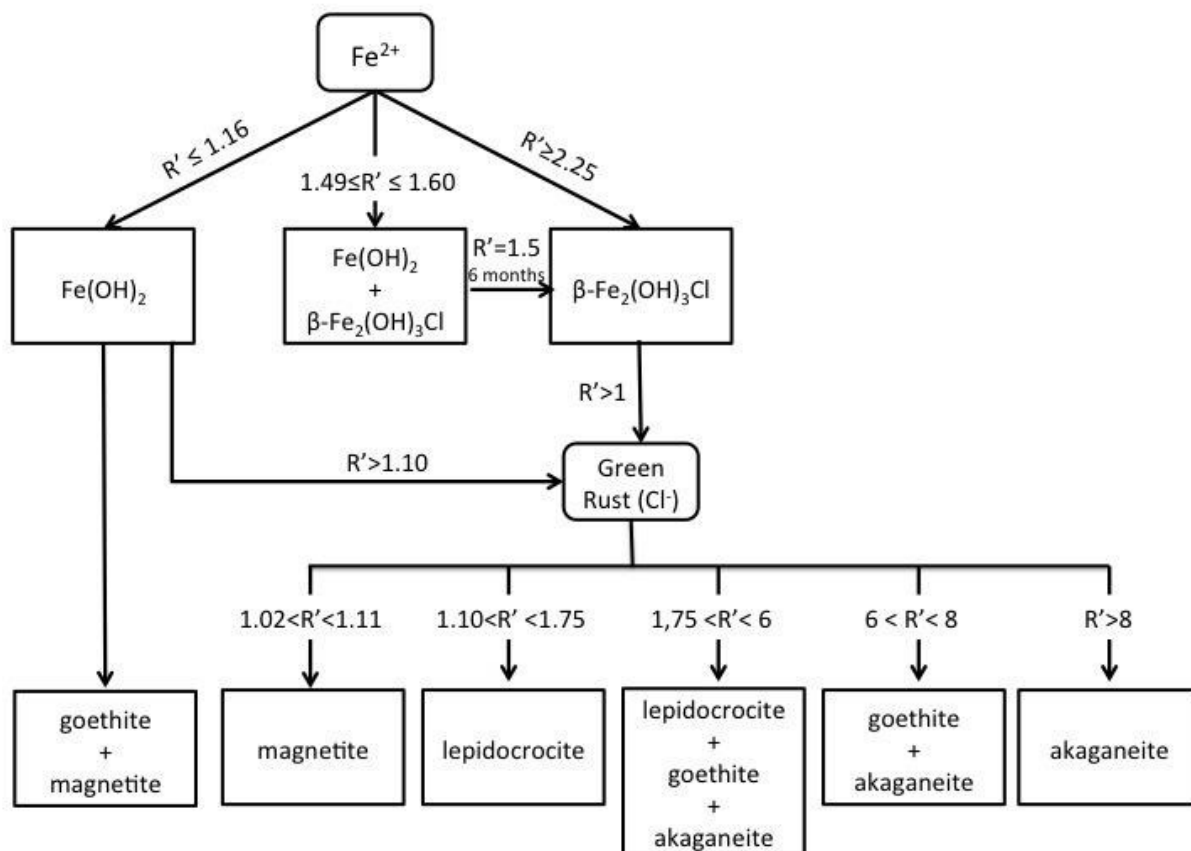


Figure 9 : Summarized diagram of phase formation during the iron oxidation process in chloride medium. $R = R'/2$, $[\text{NaOH}] = 0.4 \text{ mol.L}^{-1}$ ^{22, 23 21, 24}

Thus the following scenario can be proposed to explain the first steps of corrosion at the interface of the bar. The introduction of the solution near the rebar provokes aqueous corrosion of iron i.e. solubilisation of ferrous cations at the interface. Despite the aerated conditions, the oxidation kinetics of iron containing species is sufficiently low to allow the migration of Fe^{2+} species relatively far from the metal/binder interface during several 10 hours. Considering the concentration of chloride and former results, $\beta\text{-Fe}_2(\text{OH})_3\text{Cl}$ could have precipitated. These phases could have formed in our experiment during the humidification of the cell because we didn't observe them when the in-situ analyses begun. Here, only chlorinated green rust was observed, this observation is in good agreement with the R' value. The next step observed in-situ is the progressive disappearance of the green rust and the concomitant precipitation of akaganeite on the more internal part of the pore and goethite at the external one. In our case the absence of lepidocrocite could indicate moderated oxygen content in the solution in the observed zones because this phase is generally identified in more aerated conditions ²⁵. The presence of goethite farther from the metal/binder interface is explained by the decreasing Fe profile, favouring the precipitation of goethite. This precipitation of phases will progressively clog the porosities of the pore network, hindering the water penetration in the binder. Consequently two different consequences are observed here. The first one is linked to the presence of low-density chlorinated phases that could provoke an important cracking of the binder after precipitation. The second one is linked to the fact that iron can migrate relatively far from the interface. This will diminish the first effect significantly.

Conclusions

In-situ analyses have been performed on a cell constituted of a steel bar in a mortar matrix. The first steps of the steel bar corrosion when mortar is saturated by a chlorinated solution have been observed thanks to micro-XRF and micro-XRD. These first results highlight the presence of an intermediate Fe(II)-Fe(III) corrosion product, the chlorinated green rust which tends to transform in ferric oxyhydroxydes such as akaganeite or goethite. The nature of the precipitated phase depends on the local chloride content, the presence of dissolved O_2 and the migration of Fe^{2+} in the pore network of the binder. The presence of the transient phase could have catastrophic consequences on the structure of the binder. Actually its lower density could lead to the appearance of new cracks after its precipitation. Nevertheless, an interesting result of the in-situ measurements is that the oxidation process of Fe^{2+} species generated by the corrosion processes, is relatively slow and takes several 10 hours, during which, iron, under the form of Fe^{2+} ions can migrate several millimeters in the pore network before any precipitation. This could considerably lower the effect of the precipitation of corrosion products at the metal/binder interface and decrease the danger of cracking of the binder by this precipitation because phases can be distributed in a larger volume. Further results have to be performed with various conditions, to study the effect of different solution concentrations, especially in chloride. But these first results are a crucial step to better

understand the transient process involved in the degradation in presence of chlorides of reinforced concrete used for the building of historical monuments and more largely for any historical building reinforced by iron and steel sealed in hydraulic binder.

Acknowledgements

Authors would like to acknowledge the LabEx Patrima for the funding and DiffAbs beamline staff for the help to conduct the experiment and the CEA-LECB team for the scientific interaction on the project. We appreciated particularly the contribution of time and effort of Frederic Picca from instrumental group of SOLEIL synchrotron who helped in the XRD data treatment.

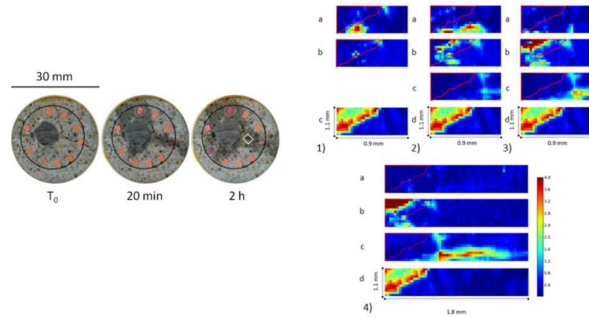
Notes and references

- ^a LAPA: NIMBE, SIS2M UMR3299 CEA/CNRS and IRAMAT UMR5060 CNRS, CEA Saclay, 91191 Gif sur Yvette Cedex, France.
- ^b L2MGC, University of Cergy-Pontoise, 95000 Cergy.
- ^c Synchrotron SOLEIL, Saint-Aubin BP48, 91192 Gif-sur-Yvette, France.
1. M. L'Héritier, P. Dillmann, A. Timbert and P. Bernardi, in *Nuts and bolt of construction history. Culture, technology and society. Vol. 2.*, ed. R. Carvais, A. Guillaume, V. Nègre and J. Sakarovitch, Picard, Paris. 2012.
2. M. L'Héritier, P. Dillmann and P. Benoit, *Historical Metallurgy*, 2010, **44**, 21-35.
3. P. Bernardi and P. Dillmann, in *De Re Metallica. The uses of metal in the Middle Ages.*, ed. R. Bork, ASHGATE. 2005, vol. 4, pp. 297-315.
4. P. Dillmann, F. Mirambet, S. Reguer and M. L'Heritier, *L'Actualité Chimique*, 2007, 71-77.
5. D. Neff, E. Marie Victoire, V. L'Hostis, E. Cailleux, L. Vincent, A. Texier, L. Bellot-Gurlet and P. Dillmann, *Metal07*, Amsterdam, Year.
6. E. Marie-Victoire, E. Cailleux and A. Texier, *Journal de Physique IV*, 2006, **136**, 305-318.
7. E. Marie-Victoire and A. Texier, *Durability of Building Materials and Components 8, Vols 1-4, Proceedings*, 1999, 581-592.
8. L. Bertolini, B. Elsener, P. Pedferri, E. Redaelli and R. B. Polder, *Corrosion of Steel in Concrete: Prevention, Diagnosis, Repair*, Wiley. 2013.
9. K. Tuuti, *Corrosion of steel in concrete*, Swedish Cement and Concrete Research Institute. 1982.
10. G. K. Glass and N. R. Buenfeld, *Corrosion Sci.*, 1997, **39**, 1001-1013.
11. A. Demoulin, C. Trigance, D. Neff, E. Foy, P. Dillmann and V. L'Hostis, *Corrosion Sci.*, 2010, **52**, 3168-3179.
12. Y. Zhao, H. Ren, H. Dai and W. Jin, *Corrosion Sci.*, 2011, **53**, 1646-1658.
13. D. Neff, J. Harnisch, M. Beck, V. L'Hostis, J. Goebbels and D. Meinel, *Materials and Corrosion*, 2011, **62**, 861-871.
14. Q. Yuan, C. Shi, G. De Schutter, K. Audenaert and D. Deng, *Construction and Building Materials*, 2009, **23**, 1-13.
15. H. S. Wong, Y. X. Zhao, A. R. Karimi, N. R. Buenfeld and W. L. Jin, *Corrosion Sci.*, 2010, **52**, 2469-2480.
16. K. Nakano, K. Akioka, T. Doi, M. Arai, H. Takabe and K. Tsuji, *ISIJ International*, 2013, **53**, 1953-1957.
17. S. Hirano, K. Akioka, T. Doi, M. Arai and K. Tsuji, *X-Ray Spectrometry*, 2014, **43**, 216-220.
18. A. Farci, D. Floris and P. Meloni, *Journal of Cultural Heritage*, 2005, **6**, 55-59.
19. F. Baudalet, R. Belkhou, V. Briois, A. Coati and P. Dumas, *Oil & Gas Science and Technology*, 2005, **60**, 849-874.

Journal Name

20. K. Medjoubi, T. Bucaille, S. Hustache, J.-F. Bézar, N. Boudet, J.-C. Clemens, P. Delpierre and B. Dinkespiler, *Journal of Synchrotron Radiation*, 2010, **17**, 486-495.
21. C. Remazeilles and P. Refait, *Corrosion Sci.*, 2008, **50**, 856-864.
22. P. Refait and J. M. R. Génin, *Corrosion Sci.*, 1997, **39**, 539-553.
23. P. Refait and J. M. R. Génin, *Corrosion Sci.*, 1993, **34**, 797-819.
24. C. Rémazeilles and P. Refait, *Corrosion Sci.*, 2007, **49**, 844-857.
25. T. Misawa, K. Hashimoto and S. Shimodaira, *Corrosion Sci.*, 1974, **14**, 131-149.

Table of contents



In-situ analyses under synchrotron XRD have highlighted the corrosion processes a rebar embedded in concrete in presence of chloride.